

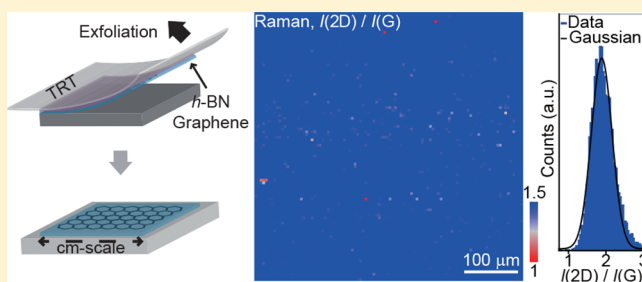
All-Dry Transfer of Graphene Film by van der Waals Interactions

Seong-Jun Yang,[†] Shinyoung Choi,[†] Francis Okello Odongo Ngome,[‡] Ki-Jeong Kim,[§] Si-Young Choi,[‡] and Cheol-Joo Kim^{*,†}[†]Department of Chemical Engineering and [‡]Department of Materials Science and Engineering, Pohang University of Science and Technology (POSTECH), Pohang, Gyeongbuk 37673, South Korea[§]Beamline Research Division, Pohang Accelerator Laboratory (PAL), Pohang, Gyeongbuk 37673, South Korea

Supporting Information

ABSTRACT: We report a method that uses van der Waals interactions to transfer continuous, high-quality graphene films from Ge(110) to a different substrate held by hexagonal boron nitride carriers in a clean, dry environment. The transferred films are uniform and continuous with low defect density and few charge puddles. The transfer is effective because of the weak interfacial adhesion energy between graphene and Ge. Based on the minimum strain energy required for the isolation of film, the upper limit of the interfacial adhesion energy is estimated to be 23 meV per carbon atom, which makes graphene/Ge(110) the first as-grown graphene film that has a substrate adhesion energy lower than that of typical van der Waals interactions between layered materials. Our results suggest that graphene on Ge can serve as an ideal material platform to be integrated with other material systems by a clean assembly process.

KEYWORDS: Dry transfer, graphene, chemical vapor deposition, adhesion energy, van der Waals interaction



Two-dimensional (2D) materials with pristine interfaces form the basis of many functional devices, including transistors, tunneling devices, and photodiodes.^{1–5} One versatile approach to realize such interfaces is a mechanical transfer technique, by which target materials of interest are mechanically exfoliated from growth substrates by van der Waals interactions with carrier films.^{6,7} This approach minimizes atomic defects in the transferred film without changing the in-plane covalent bonds. Additionally, it can preserve clean interfaces of the film by preventing exposure to wet chemicals, which leave ionic and metal impurities.⁸ van der Waals interaction assisted transfer was recently demonstrated with wafer-scale monolayer transition metal dichalcogenides films grown on silicon oxides and has successfully provided large-scale 2D semiconductors with high quality interfaces.⁷ However, application of the technique to another important element, graphene, is still limited to micrometer-size samples,⁶ and fabrication of large-scale graphene devices with pristine interfaces remains challenging.

The difficulty in scaling up the mechanical transfer arises from lack of large-scale graphene samples, which are feasible to exfoliate from the substrates. In particular, the interactions between graphene and carrier film need to overcome the adhesive force of graphene to the underlying substrate. Graphene films grown on typical substrates including Cu and SiC do not satisfy the condition.^{9,10} The films adhere to the substrates with adhesion energies (γ) of 60 meV/carbon (C) atom on Cu¹¹ and 106 meV/C atom on SiC,¹⁰ which are

significantly higher than typical van der Waals interactions, which have $40 \leq \gamma \leq 50$ meV/C atom between graphene and other layered materials.^{12,13} As a result, mechanical transfer by van der Waals forces achieves low yield. To overcome this problem, previous research has used carriers that have stronger adhesions to graphene than to the substrate; the carriers have included polymers that have covalent links and metals that have strong electrostatic interactions. However, these methods require undesirable wet etching of the carriers.^{10,14}

In this report, we present an all-dry mechanical transfer method for large-scale graphene films by nondestructive van der Waals interactions with hexagonal boron nitride (*h*-BN) carrier films. The key aspect of our developments is to provide easily detachable graphene films. We achieve the goal by growing graphene on Ge(110) substrates.^{15,16} Due to a weak adhesion to the substrate, the graphene film can be effectively exfoliated and transferred while being attached to a *h*-BN superlayer by van der Waals interactions. The transferred films are uniform and continuous with low density of defects and few charge puddles. The results suggest that our method provides a versatile, clean, and scalable way to engineer interfaces of graphene.

Our transfer method (Figure 1a; Supporting Information) entails four main steps: (i) a high-quality graphene film with

Received: February 7, 2019

Revised: April 26, 2019

Published: May 13, 2019

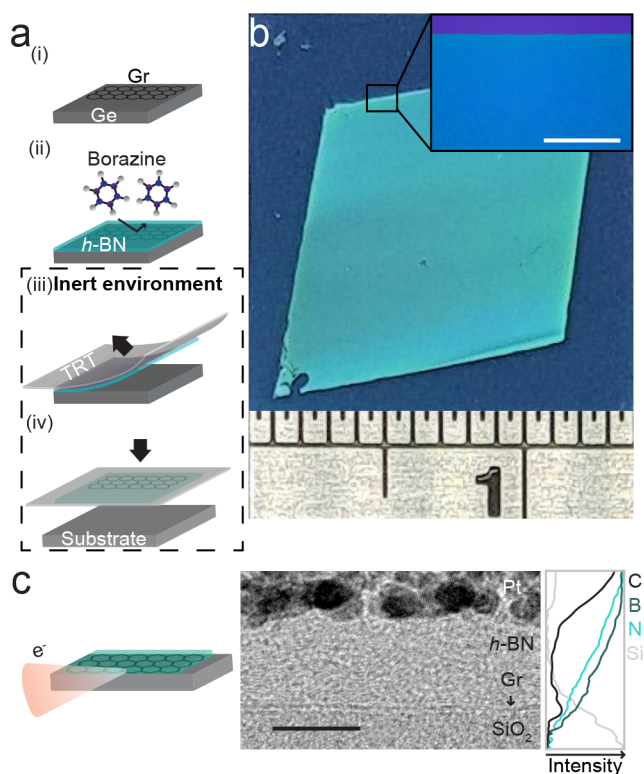


Figure 1. (a) Schematics of the all-dry transfer process of graphene film by van der Waals interactions: (i) graphene growth on Ge(110), (ii) *h*-BN growth, (iii) mechanical exfoliation of *h*-BN/graphene hybrid film by TRT, and (iv) transfer of the film to arbitrary substrates. (b) Optical image of 50 nm *h*-BN/graphene film transferred onto a SiO₂/Si substrate. Scale bar: 100 μm. (c) (left) Schematics for cross-sectional TEM, (middle) TEM image, and (right) EDX intensity profile for carbon, boron, nitrogen, and silicon elements. Scale bar: 10 nm.

uniform thickness is grown on a Ge(110) substrate by chemical vapor deposition (CVD), (ii) a *h*-BN carrier film is subsequently grown on the top surface of graphene, (iii) the whole *h*-BN/graphene composite film is mechanically exfoliated using a thermal-release tape (TRT), and (iv) it is then transferred onto a target substrate in an inert environment.

We chose Ge(110) substrate and *h*-BN carrier materials to ensure high transfer yield and cleanliness at the graphene interfaces. Ge(110) is a good template to grow a weakly bonded graphene film for feasible exfoliations because it has a dissimilar lattice structure to graphene and low free carrier concentration to suppress electrostatic interactions.¹⁷ Adhesion of graphene is significantly weaker to Ge(110) than to other growth substrates.¹⁶ Here, we test whether the adhesion is even weaker than van der Waals interactions between graphene and other layered materials; if so, the weak adhesion would enable mechanical transfer assisted by van der Waals interaction. For that purpose, we grew *h*-BN films on graphene and used them as carriers. The surface of *h*-BN has no dangling bonds, so it has minimal effect on the electrical properties of graphene. Therefore, we do not need to remove *h*-BN, so interfaces of graphene remain clean.

We first checked the feasibility of the transfer by optically examining the films at macroscopic scales. An optical image (Figure 1b) of a centimeter-sized *h*-BN/graphene film transferred onto a 300 nm silicon dioxide/silicon (SiO₂/Si)

substrate shows uniform optical contrast over the whole area compared to the bare SiO₂/Si substrate; this uniformity demonstrates transfer of a continuous, homogeneous film without wrinkles or cracks. To identify the contents of the transferred film, energy-dispersive X-ray (EDX) elemental map was obtained by transmission electron microscopy (TEM) in a 50 nm thin slide of 10 nm *h*-BN/graphene on a SiO₂/Si substrate that was carved out using a focused ion beam. The EDX intensity profiles (Figure 1c) for each element, including carbon, boron, nitrogen, and silicon, across the interfaces clearly identify both *h*-BN and graphene layers on the SiO₂ surface. Also, optical absorption spectra were measured with a beam diameter of 0.5 cm in a film transferred onto a fused silica substrate (Supporting Information, Figure S1), and the presences of both *h*-BN and graphene films were confirmed over the large area by their optical spectra signatures.

The transfer yield was confirmed by using spatially resolved characterizations after each stage of the process (Figure 1a) to observing the structural homogeneity of the films. Our method achieved almost 100% transfer of as-grown graphene films with ultraflat surfaces and low density of atomic defects while preserving excellent structural homogeneity with uniform monolayer thickness and low density of atomic defects throughout the processes. First, atomic force microscopy (AFM) height image of an as-grown graphene sample (Figure 2a) shows an ultraflat surface with a few terrace structures of atomic steps. While nanoscale particles are observed in the film, their formations can be suppressed if the Ge substrate undergoes a precleaning process before the growth of graphene (Supporting Information, Figure S2). Low energy electron diffraction (LEED) pattern (Figure 2a, inset) and Raman spectra image with 488 nm excitation wavelength (Supporting Information, Figure S3) confirmed the uniform monolayer thickness and the low density of atomic defects. The high-quality samples were provided for subsequent CVD of *h*-BN carrier films. An optical image (Figure 2b) of a *h*-BN/graphene film on a Ge(110) substrate was obtained after exfoliation of only the right side of the sample (Supporting Information, Figure S4). Raman spectra of the as-grown region (Figure 2b, right panel) shows clear G and 2D peaks of graphene and the E_{2g} peak of *h*-BN (1373 cm⁻¹) but not in spectra of the exfoliated region. Raman intensity maps of graphene 2D peak (Figure 2b, bottom panel) further demonstrate effective exfoliation of the film. In the as-grown region, the 2D peak intensity shows a variation of ±33% of the average value over the scanned region, possibly due to the inhomogeneous strain on graphene film.¹⁷ Nonetheless, we found that the subsequent *h*-BN growth does not introduce significant graphene Raman D peak associated with atomic defects if the initial graphene film has a uniformly high Raman 2D intensity (Supporting Information, Figures S5 and S6). Finally, we transferred the film onto a SiO₂/Si substrate and obtained a 2D/G Raman peak intensity ratio map (Figure 2c). The 2D/G intensity ratio is spatially uniform; the distribution has a single Gaussian peak with an average value of 1.9 (Figure 2c, right panel), and this result indicates that the graphene was a uniform monolayer (Supporting Information, Figure S7).¹⁸

To check whether the transfer process induces contamination to graphene, we examined the bottom surface of exfoliated graphene film by using X-ray photoelectron spectroscopy (XPS) (Figure 2d, upper schematics). Apparent Ge 3d peaks from the as-grown sample (Figure 2d, left-most inset) are totally absent from graphene after its isolation from a

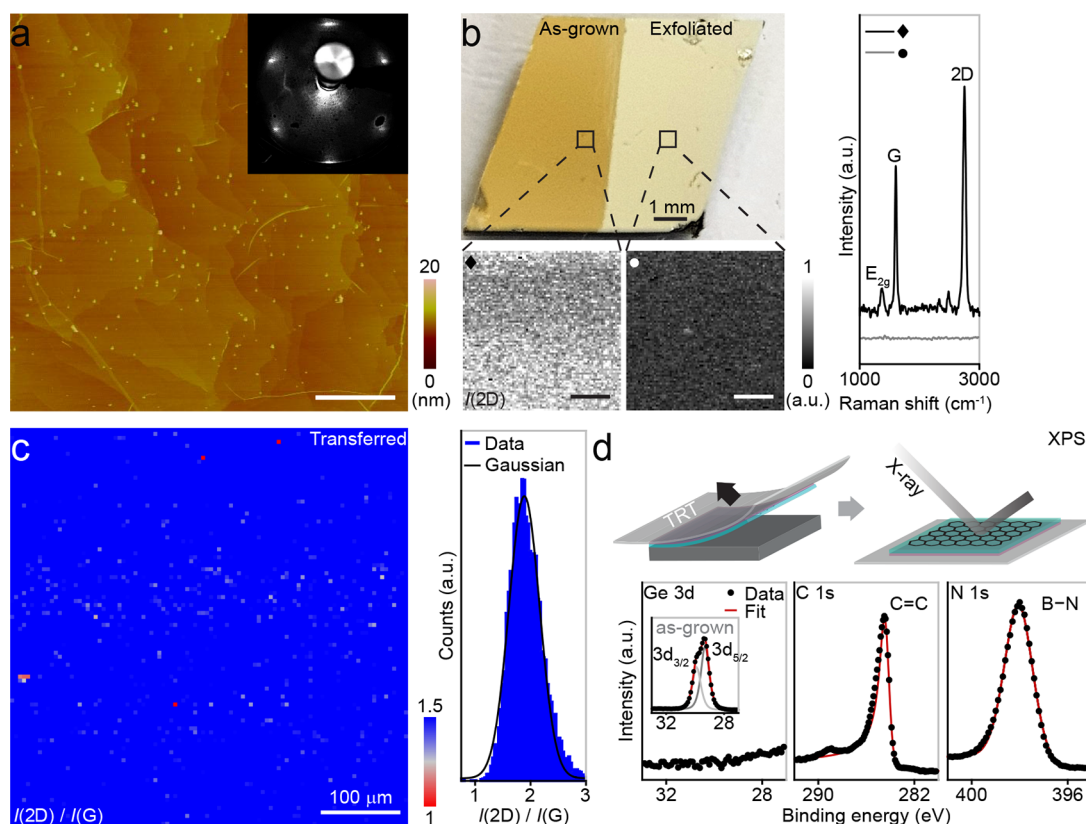


Figure 2. (a) (Main panel) AFM height image and (inset) LEED pattern measured from a graphene film grown on a Ge(110) substrate. Scale bar: 1 μm . (b) Photograph of a 45 nm *h*-BN/graphene hybrid film on a Ge(110) substrate, where only the right side of the film is exfoliated for comparison. Left-bottom images: Raman intensity maps for graphene 2D peak measured from the squared regions of the (diamond) as-grown and (circle) exfoliated parts. Right panel: Each Raman spectrum. Scale bars: 10 μm . (c) (left) 2D/G Raman peak intensity ratio map of 20 nm *h*-BN/graphene film transferred onto a SiO_2/Si substrate and (right) distribution of the ratios. (d) (Top) Schematics for XPS measurements and (bottom: left to right) XPS spectra for Ge 3d, C 1s, and N 1s peaks.

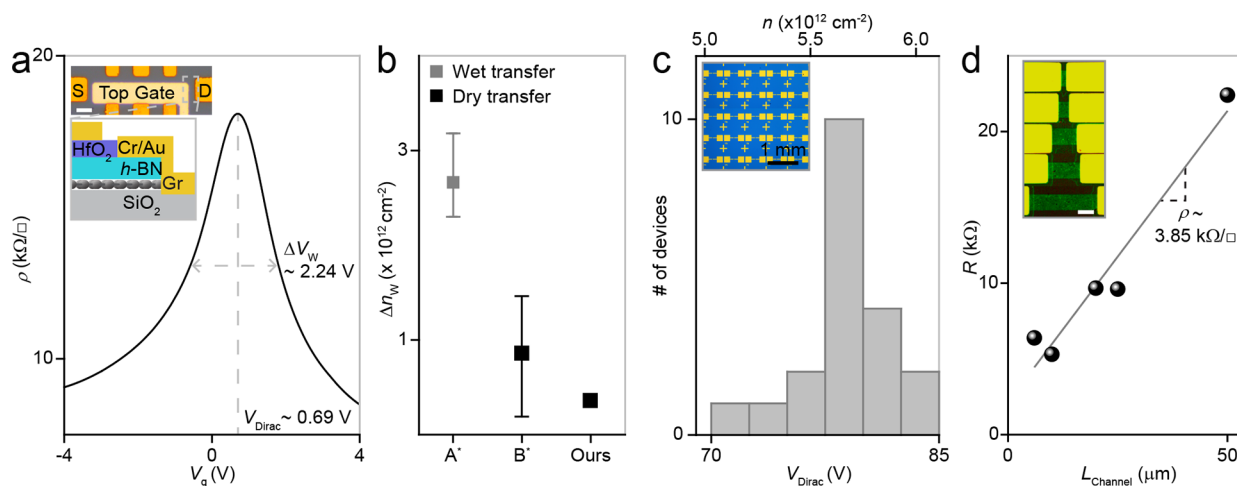


Figure 3. (a) Top gate voltage-dependent sheet resistivity of a 65 nm *h*-BN/graphene channel on a fused silica substrate. Inset: optical image and a schematic for the device. Scale bar: 10 μm . (b) Inhomogeneous charge variations for different graphene channels deduced from Dirac peak widths based on a capacitance model. A^* and B^* are extracted from refs 26 and 25, respectively. (c) Distribution of Dirac voltages and corresponding doping levels measured at (inset) 50 nm *h*-BN/graphene channel arrays on a SiO_2/Si substrate. (d) Channel length dependent resistances of 50 nm *h*-BN/graphene channels with different lengths. All the graphene samples are prepared by the all-dry transfer method. Scale bar: 10 μm .

Ge substrate (Figure 2d, left-most spectra). Over the full energy range of XPS measurement from 0 to 1300 eV, signals associated with metal elements are absent; this result indicates that the surface is free of metal impurities (Supporting Information, Figure S8). In contrast, C 1s peaks are mostly

preserved; the main peak at 284.4 eV is assigned to carbons that have a graphitic sp^2 bond.^{19,20} Furthermore, the cross-sectional TEM image on a transferred film (Figure 1c) does not show contamination bubbles with few tens of nanometers in size at the interfaces, which are evidently observed in

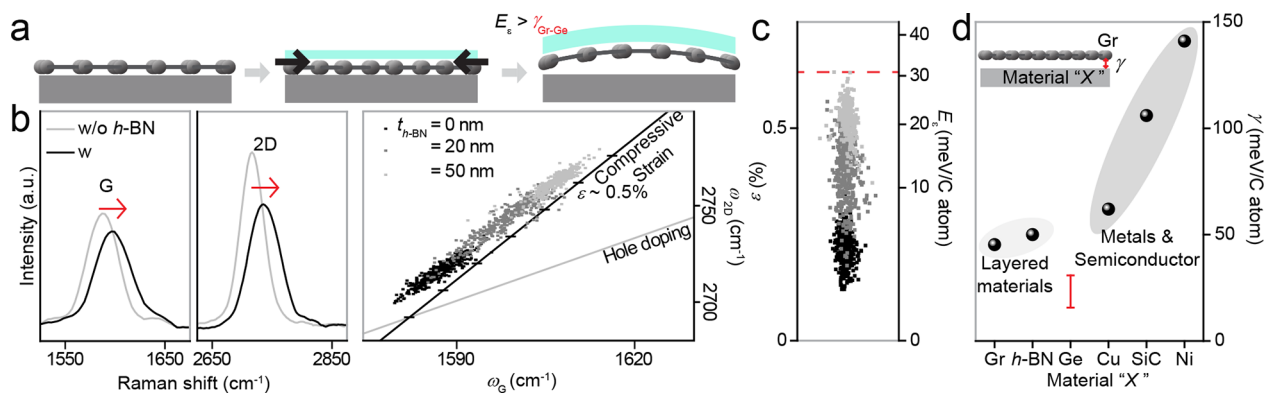


Figure 4. (a) Schematics of buckling of graphene film induced by compressive strain by superlayer deposition. When residual strain energy (E_e) exceeds the interfacial adhesion energy ($\gamma_{\text{Gr-Ge}}$) between graphene and the substrate, spontaneous buckling can occur. (b) Left: Representative Raman spectra for graphene G and 2D peaks before and after *h*-BN depositions. The excitation wavelength is 488 nm; right: 2D peak positions (ω_{2D}) versus G peak positions (ω_G) measured at multiple spots of samples with different *h*-BN thicknesses. Overlain lines: compressive strain (black) and hole doping (gray) dependent ω_{2D} and ω_G taken from previous studies.^{29,30} (c) Compressive strain and corresponding E_e of graphene films from Figure 4b, deduced by ω_{2D} and ω_G . Red dotted line: maximum value of strain and E_e ; i.e., at critical thickness. (d) Interfacial adhesion energy between graphene and other materials from previous reports (graphene,¹² *h*-BN,¹³ Cu,¹¹ SiC,¹⁰ and Ni¹¹). $\gamma_{\text{Gr-Ge}}$ is deduced from the maximum E_e in Figure 4c.

abundance in samples that are transferred by a method involving wet processes to etch polymer and metallic supporting films.^{8,21} While the possibility of airborne contaminations at an atomic level cannot be completely ruled out in the current stage,²² the lack of hydrocarbon and metal-related features in TEM and XPS measurements suggests that contaminations are substantially reduced at nanometer scales by all-dry transfer method. Randomly distributed ionic or metal impurities cause inhomogeneous doping effects and result in nonuniform electrical properties of graphene devices. These effects hamper realizations of novel phenomena and applications of graphene devices.^{4,6,23} Our transfer method can eliminate these limitations by providing clean and defect-free graphene channels for electronic devices, as demonstrated below.

We fabricated (Supporting Information) field-effect transistors (FETs) based on graphene films transferred by the all-dry method and then evaluated their electrical properties. The graphene channels were protected by a *h*-BN superlayer throughout the fabrication processes, and only the edges of graphene were exposed to make electrical contacts.⁶ The structure and dielectric properties of *h*-BN films, which are used as a protective layer and a gate dielectric layer, are characterized by TEM, AFM, and capacitance measurements (Supporting Information). Consequently, *h*-BN films show amorphous-like structures with nanometer size domains (Figure S9) with the dielectric constant of 2 and the breakdown field of 0.5 MV/cm (Figure S10), similar to the properties of previously reported multilayer films grown by chemical vapor deposition.²⁴ For a *h*-BN/graphene channel on a fused silica (Figure 3a, inset), sheet resistivity (ρ) at room temperature varied as a function of the top gate voltage (V_g). By measuring the full width at half-maximum (ΔV_w) of ρ near the charge-neutral point, we estimate the upper limit of inhomogeneous charge puddle (Δn_w) at the low doping level by using a simple capacitance model $\Delta n_w = \Delta V_w C_g / e$, where C_g is the gate capacitance per unit area and e is the elementary charge. The estimated value is $\Delta n_w = 3.6 \times 10^{11} \text{ cm}^{-2}$, which is comparable to the smallest values measured by the same method from small flakes on SiO_2/Si substrates²⁵ and much

smaller than the values from wet-transferred films (Figure 3b).²⁶

We also measured transconductance of an array of FETs with back-gated structures on a SiO_2/Si substrate (Figure 3c) by batch fabrication. On an SiO_2/Si substrate, the graphene channels show typical *p*-type doping characteristics with the charge-neutral V_g (V_{Dirac}) at high positive voltages, similar to previous reports. Our measured V_{Dirac} had a small variation within 10^{12} cm^{-2} , which is comparable to the doping inhomogeneity induced by charge puddles in clean graphene films on SiO_2/Si substrates.²⁷ The observation suggests that the doping homogeneity is mainly determined by the surface structure rather than by contamination caused by the transfer process and that homogeneity in the sample is maintained from micrometer scale to centimeter scale. As a result, graphene channels with different lengths have well-defined resistivity at zero V_g (Figure 3d). The electrical properties, especially the carrier mobility, can still be improved (Supporting Information, Figure S11). Nevertheless, our results demonstrate that this all-dry transfer process based on graphene/Ge(110) provides uniform films without additional disorders.⁴

The effective transfer indicates that adhesion energy between graphene and Ge(110) ($\gamma_{\text{Gr-Ge}}$) is indeed weaker than the van der Waals interactions between graphene and *h*-BN interfaces. Here, we further measure $\gamma_{\text{Gr-Ge}}$ quantitatively to provide a useful guideline to evaluate the feasibility of graphene transfer by other materials beside *h*-BN. To estimate $\gamma_{\text{Gr-Ge}}$ we measured the strain energy (E_e) required to exfoliate graphene films from Ge substrates. When *h*-BN superlayer is deposited on graphene to more than a critical thickness of 50 nm, the *h*-BN/graphene films spontaneously delaminated with buckling (Supporting Information, Figure S12). This phenomenon typically happens when compressive residual E_e exceeds $\gamma_{\text{Gr-Ge}}$ (schematics in Figure 4a).²⁸ By using micro-Raman spectroscopy, we tried to monitor the accumulative compressive strain in the graphene films as *h*-BN superlayers thickened until the strain was released by the spontaneous delamination. Raman spectra (Figure 4b) near G and 2D peaks of graphene measured before and after deposition of *h*-BN superlayers show blue shifts in both peaks after the deposition; the shifts

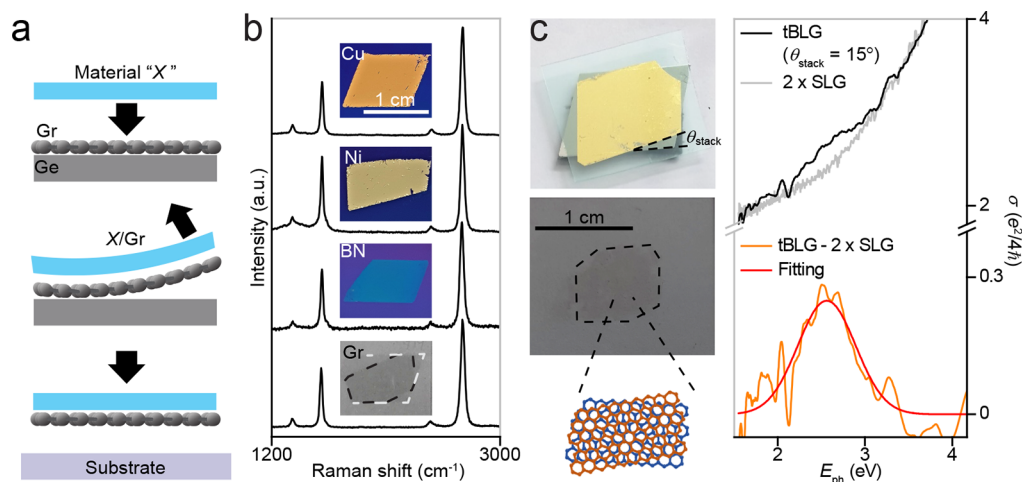


Figure 5. (a) Schematics for a “contact and peel” process to fabricate graphene films interfaced with arbitrary material X. (b) (inset, top to bottom) Photographs of X/graphene films ($X = \text{Cu}$, Ni , $h\text{-BN}$, and graphene) transferred onto SiO_2/Si or fused silica substrates and (main panel) corresponding Raman spectra. Metal superlayers were chemically removed for the Raman measurements. (c) (left, from top to bottom) Photograph of stacked tBLG with $\theta_{\text{stack}} = 15^\circ$ on Ge, transferred tBLG on fused silica and schematics of tBLG. (right) Measured optical conductivity (σ) spectra of tBLG with $\theta_{\text{stack}} = 15^\circ$ (σ_{tBLG} , black), $2 \times \sigma$ spectra of single-layer graphene ($2 \times \sigma_{\text{SLG}}$, gray), and $\sigma_{\text{tBLG}} - 2 \times \sigma_{\text{SLG}}$ (orange).

increased as the thickness of $h\text{-BN}$ film increased (Figure 4b, right panel). We compared our data with previous reports, where the peak shifts are measured as a function of two dominant factors for phonon stiffening of graphene, i.e., compressive strain and hole doping (Figure 4b, right panel).^{29,30} 2D peak position (ω_{2D}) and G peak position (ω_G) changed in response to compressive strain. The compressive strain was deconvoluted using a simple equation based on linear combinations of peak shifts caused by the two dominant factors; the deduced strain shows a maximum value of about 0.67% in the samples with $h\text{-BN}$ films above the critical thickness.

Based on the maximum strain values measured from multiple samples, we deduce the maximum E_e in $h\text{-BN}/\text{graphene}$ film prior to the delamination. According to fracture mechanics,^{28,31} the E_e is considered to be equivalent to $\gamma_{\text{Gr-Ge}}$ when all E_e is applied to overcome $\gamma_{\text{Gr-Ge}}$ for the delamination. $E_e = \epsilon^2 E_{\text{Gr}} t_{\text{Gr}} / (1 - \nu_{\text{Gr}})$, where ϵ , E_{Gr} , t_{Gr} , and ν_{Gr} are, respectively, the strain, Young’s modulus, thickness, and Poisson ratio of graphene, if most of the residual strain is accumulated at graphene, which is significantly softer than the much thicker $h\text{-BN}$ superlayer. The calculation yielded $\gamma_{\text{Gr-Ge}} = 23 \pm 7.5$ meV/C atom (Figure 4d). This value is considered as the upper limit of $\gamma_{\text{Gr-Ge}}$. In reality, not all of E_e is used for the delamination, so a residual stress remains in the final film (Supporting Information, Figure S12). The calculated $\gamma_{\text{Gr-Ge}}$ is the smallest ever reported for interfacial adhesion energies between an as-grown graphene film and a growth substrate.^{10,11} The value is even smaller than the γ of van der Waals interactions between layered materials; this conclusion is consistent with the high yield transfer of graphene by interaction with $h\text{-BN}$ superlayer.¹³

The feasibly detachable graphene on Ge(110) further enables a general “contact and peel” approach (Figure 5a) to produce transferable graphene films with engineered top interfaces. In detail, one can stack arbitrary material X other than $h\text{-BN}$ on the top surface of as-grown graphene film, either by deposition or by transfer of X to form clean X/graphene interfaces. Then, the composite films can be peeled and

transferred onto arbitrary substrates to exploit the properties of X/graphene interfaces. The interfaces are formed in an inert environment, so pristine interfaces should be obtained without oxidation of X. Moreover, the whole film can be transferred onto arbitrary substrates, so the properties of X/graphene composites can be studied without any effects from the growth substrate. This approach can be applied to fabricate various interfaces at a high production yield as long as $\gamma_{\text{Gr-Ge}}$ is weakest among the all interlayer adhesions in the stacked composite films before exfoliation, and facilitates fabrication of devices by integrating other material components.

By applying the “contact and peel” approach to as-grown graphene film on Ge(110), we fabricated (Supporting Information) transferable graphene films interfaced with arbitrary material X ($X = \text{Cu}$, Ni , $h\text{-BN}$, and graphene) and then transferred the films onto target substrates (Figure 5b, inset). Raman spectra of all samples (Figure 5b) show clear G and 2D peaks of single-layer graphene, confirming successful formation and transfer of X/graphene interfaces. In particular, we can fully isolate graphene film on Ge(110) by stacking another graphene film on top and then exfoliating the stacked double-layer graphene to realize layer-by-layer assembly of 2D materials. In this approach, as the individual graphene films have aligned crystalline structure (Figure 2a, inset), twisted bilayer graphene (tBLG) with a controlled interlayer rotational angle (θ_{stack}) can be fabricated (Figure 5c, left panel). As an example, tBLG with $\theta_{\text{stack}} = 15^\circ$ is fabricated, and the real part of optical conductivity (σ) is deduced from optical transmission measurements.³² The measured σ from tBLG (σ_{tBLG}) shows twice the value of σ from single-layer graphene (σ_{SLG}) in most of the spectral range, proving effective formation and transfer of tBLG. When the value of σ_{tBLG} spectra (Figure 5c, black) is subtracted by twice the value of σ_{SLG} spectra (Figure 5c, gray), an extra absorption peak (Figure 5c, orange) is observed at 2.56 eV. This energy is close to the interband transition energy of 2.6 eV between van Hove singularities resulting from the interlayer interactions between the two graphene layers with $\theta = 15^\circ$. To check the interlayer coupling efficiency, we compared the integrated absorption peak

intensity with the value measured from as-grown tBLG with clean interfaces.³² The integrated absorption peak intensity is comparable to the reference value, suggesting a formation of clean interfaces with efficient interlayer interactions (Supporting Information, Figure S13).

In summary, we report that graphene films grown on Ge(110) are transferable by van der Waals interactions with supporting superlayers in an all-dry environment. Our results demonstrate that graphene films on Ge(110) can serve as an ideal component for a versatile assembly process to integrate graphene with other material systems.^{33,34} In particular, recent studies have shown that Ge can also serve as a growth substrate for other layered materials. For example, Ge(100) and Ge(110) can facilitate the growth of semiconducting graphene nanoribbons and insulating *h*-BN monolayer on their surfaces. Apparently, the adhesion energies of the materials to the underlying Ge are weak, at least below 60 meV/C atom.^{35,36} The weak adhesion implies that our all-dry transfer method on Ge substrate can be applied to the atomically thin layered materials, enabling the assembly of complex structures with more building blocks. The approach will be useful for realizing large-scale 2D electronics and for discovering new hybrid materials that have novel electrical and optical properties.^{37–40}

■ ASSOCIATED CONTENT

Supporting Information

The Supporting Information is available free of charge on the ACS Publications website at DOI: [10.1021/acs.nanolett.9b00555](https://doi.org/10.1021/acs.nanolett.9b00555).

Experimental methods for CVD of graphene on Ge(110) substrate, all-dry transfer process of graphene film, TEM sample fabrication and characterization, dielectric property characterization of *h*-BN films, device fabrication and “contact and peel” process, supporting data for optical absorption spectra of transferred *h*-BN/graphene hybrid film, AFM height images of graphene film on Ge with different chemical treatments, Raman spectra of graphene film on Ge(110), all-dry transfer process of graphene film, Raman spectra change in the defective graphene film after *h*-BN growth, Raman spectra change in the high-quality graphene film after *h*-BN growth, Raman spectra of multilayer graphene film, X-ray photoelectron spectroscopy on an exfoliated graphene surface, structural characterization of *h*-BN films, dielectric properties of *h*-BN films, field-effect carrier mobility of graphene channels, calculation of interfacial toughness between graphene and Ge(110) based on the geometry of formed buckles, and interlayer optical absorption peak area in artificially fabricated tBLG (PDF)

■ AUTHOR INFORMATION

Corresponding Author

*E-mail: kimcj@postech.ac.kr; Phone: +82-54-279-5233.

ORCID

Ki-Jeong Kim: [0000-0001-9233-3096](https://orcid.org/0000-0001-9233-3096)

Cheol-Joo Kim: [0000-0002-4312-3866](https://orcid.org/0000-0002-4312-3866)

Notes

The authors declare no competing financial interest.

■ ACKNOWLEDGMENTS

We thank J. Park for experimental help. This research was supported by the International Research & Development Program (NRF-2017K1A3A1A12073407) and the Creative Materials Discovery Program (NRF-2018M3D1A1058793) of the National Research Foundation of Korea (NRF) funded by the Ministry of Science, ICT & Future Planning, as well as the Basic Science Research Program through the NRF funded by the Ministry of Education (NRF-2017R1D1A1B03034896). Experiments at PLS-II were supported in part by MSICT and POSTECH. Additional funding was provided by POSTECH Basic Science Research Institute. S.Y.C. is supported by the Global Frontier R&D Program on Center for Hybrid Interface Materials (HIM) funded by the Ministry of Science, ICT & Future Planning Korea (NRF-2013M3A6B1078872).

■ REFERENCES

- (1) Britnell, L.; Gorbachev, R. V.; Jalil, R.; Belle, B. D.; Schedin, F.; Mishchenko, A.; Georgiou, T.; Katsnelson, M. I.; Eaves, L.; Morozov, S. V.; Peres, N. M. R.; Leist, J.; Geim, A. K.; Novoselov, K. S.; Ponomarenko, L. A. Field-Effect Tunneling Transistor Based on Vertical Graphene Heterostructures. *Science* **2012**, *335*, 947–950.
- (2) Yang, H.; Heo, J.; Park, S.; Song, H. J.; Seo, D. H.; Byun, K. E.; Kim, P.; Yoo, I.; Chung, H. J.; Kim, K. Graphene Barristor, a Triode Device with a Gate-Controlled Schottky Barrier. *Science* **2012**, *336*, 1140–1143.
- (3) Cobas, E.; Friedman, A. L.; van’T Erve, O. M. J.; Robinson, J. T.; Jonker, B. T. Graphene as a Tunnel Barrier: Graphene-Based Magnetic Tunnel Junctions. *Nano Lett.* **2012**, *12*, 3000–3004.
- (4) Goossens, S.; Navickaite, G.; Monasterio, C.; Gupta, S.; Piqueras, J. J.; Pérez, R.; Burwell, G.; Nikitskiy, I.; Lasanta, T.; Galán, T.; Puma, E.; Centeno, A.; Pesquera, A.; Zurutuza, A.; Konstantatos, G.; Koppens, F. Broadband Image Sensor Array Based on Graphene–CMOS Integration. *Nat. Photonics* **2017**, *11*, 366–371.
- (5) Song, K.; Soriano, D.; Cummings, A. W.; Robles, R.; Ordejón, P.; Roche, S. Spin Proximity Effects in Graphene/Topological Insulator Heterostructures. *Nano Lett.* **2018**, *18*, 2033–2039.
- (6) Wang, L.; Meric, I.; Huang, P. Y.; Gao, Q.; Gao, Y.; Tran, H.; Taniguchi, T.; Watanabe, K.; Campos, L. M.; Muller, D. A.; Guo, J.; Kim, P.; Hone, J.; Shepard, K. L.; Dean, C. R. One-Dimensional Electrical Contact to a Two-Dimensional Material. *Science* **2013**, *342*, 614–617.
- (7) Kang, K.; Lee, K. H.; Han, Y.; Gao, H.; Xie, S.; Muller, D. A.; Park, J. Layer-by-Layer Assembly of Two-Dimensional Materials into Wafer-Scale Heterostructures. *Nature* **2017**, *550*, 229–233.
- (8) Lin, Y. C.; Lu, C. C.; Yeh, C. H.; Jin, C.; Suenaga, K.; Chiu, P. W. Graphene Annealing: How Clean Can It Be? *Nano Lett.* **2012**, *12*, 414–419.
- (9) Banszerus, L.; Schmitz, M.; Engels, S.; Dauber, J.; Oellers, M.; Haupt, F.; Watanabe, K.; Taniguchi, T.; Beschoten, B.; Stampfer, C. Ultrahigh-Mobility Graphene Devices from Chemical Vapor Deposition on Reusable Copper. *Sci. Adv.* **2015**, *1*, e1500222.
- (10) Kim, J.; Park, H.; Hannon, J. B.; Bedell, S. W.; Fogel, K.; Sadana, D. K.; Dimitrakopoulos, C. Layer-Resolved Graphene Transfer via Engineered Strain Layers. *Science* **2013**, *342*, 833–836.
- (11) Hamada, I.; Otani, M. Comparative van der Waals Density-Functional Study of Graphene on Metal Surfaces. *Phys. Rev. B: Condens. Matter Mater. Phys.* **2010**, *82*, 153412.
- (12) Zacharia, R.; Ulbricht, H.; Hertel, T. Interlayer Cohesive Energy of Graphite from Thermal Desorption of Polyaromatic Hydrocarbons. *Phys. Rev. B: Condens. Matter Mater. Phys.* **2004**, *69*, 155406.
- (13) Giovannetti, G.; Khomyakov, P. A.; Brocks, G.; Kelly, P. J.; van den Brink, J. Substrate-Induced Band Gap in Graphene on Hexagonal Boron Nitride: *Abinitio* Density Functional Calculations. *Phys. Rev. B: Condens. Matter Mater. Phys.* **2007**, *76*, 073103.

- (14) Yoon, T.; Shin, W. C.; Kim, T. Y.; Mun, J. H.; Kim, T. S.; Cho, B. J. Direct Measurement of Adhesion Energy of Monolayer Graphene As-Grown on Copper and Its Application to Renewable Transfer Process. *Nano Lett.* **2012**, *12*, 1448–1452.
- (15) Wang, G.; Zhang, M.; Zhu, Y.; Ding, G.; Jiang, D.; Guo, Q.; Liu, S.; Xie, X.; Chu, P. K.; Di, Z.; Wang, X. Direct Growth of Graphene Film on Germanium Substrate. *Sci. Rep.* **2013**, *3*, 2465.
- (16) Lee, J. H.; Lee, E. K.; Joo, W. J.; Jang, Y.; Kim, B. S.; Lim, J. Y.; Choi, S. H.; Ahn, S. J.; Ahn, J. R.; Park, M. H.; Yang, C. W.; Choi, B. L.; Hwang, S. W.; Whang, D. Wafer-Scale Growth of Single-Crystal Monolayer Graphene on Reusable Hydrogen-Terminated Germanium. *Science* **2014**, *344*, 286–289.
- (17) Kiraly, B.; Jacobberger, R. M.; Mannix, A. J.; Campbell, G. P.; Bedzyk, M. J.; Arnold, M. S.; Hersam, M. C.; Guisinger, N. P. Electronic and Mechanical Properties of Graphene-Germanium Interfaces Grown by Chemical Vapor Deposition. *Nano Lett.* **2015**, *15*, 7414–7420.
- (18) Ferrari, A. C.; Basko, D. M. Raman Spectroscopy as a Versatile Tool for Studying the Properties of Graphene. *Nat. Nanotechnol.* **2013**, *8*, 235–246.
- (19) Díaz, J.; Paolicelli, G.; Ferrer, S.; Comin, F. Separation of the sp^3 and sp^2 Components in the C1s Photoemission Spectra of Amorphous Carbon Film. *Phys. Rev. B: Condens. Matter Mater. Phys.* **1996**, *54*, 8064–8069.
- (20) Moulder, J. F.; Stickle, W. F.; Sobol, P. E.; Bomben, K. D. *Handbook of X-Ray Photoelectron Spectroscopy: A Reference Book of Standard Spectra for Identification and Interpretation of XPS Data*; Chastain, J., Ed.; Perkin-Elmer Corporation Physical Electronics Division: MN, 1992.
- (21) Haigh, S. J.; Gholinia, A.; Jalil, R.; Romani, S.; Britnell, L.; Elias, D. C.; Novoselov, K. S.; Ponomarenko, L. A.; Geim, A. K.; Gorbachev, R. Cross-Sectional Imaging of Individual Layers and Buried Interfaces of Graphene-Based Heterostructures and Superlattices. *Nat. Mater.* **2012**, *11*, 764–767.
- (22) Li, Z.; Wang, Y.; Kozbial, A.; Shenoy, G.; Zhou, F.; McGinley, R.; Ireland, P.; Morganstein, B.; Kunkel, A.; Surwade, S. P.; Li, L.; Liu, H. Effect of Airborne Contaminants on the Wettability of Supported Graphene and Graphite. *Nat. Mater.* **2013**, *12*, 925–931.
- (23) Dean, C. R.; Young, A. F.; Meric, I.; Lee, C.; Wang, L.; Sorgenfrei, S.; Watanabe, K.; Taniguchi, T.; Kim, P.; Shepard, K. L.; Hone, J. Boron Nitride Substrates for High-Quality Graphene Electronics. *Nat. Nanotechnol.* **2010**, *5*, 722–726.
- (24) Kim, K. K.; Hsu, A.; Jia, X.; Kim, S. M.; Shi, Y.; Dresselhaus, M.; Palacios, T.; Kong, J. Synthesis and Characterization of Hexagonal Boron Nitride Film as a Dielectric Layer for Graphene Devices. *ACS Nano* **2012**, *6*, 8583–8590.
- (25) Bolotin, K. I.; Sikes, K. J.; Jiang, Z.; Klima, M.; Fudenberg, G.; Hone, J.; Kim, P.; Stormer, H. L. Ultrahigh Electron Mobility in Suspended Graphene. *Solid State Commun.* **2008**, *146*, 351–355.
- (26) Petrone, N.; Dean, C. R.; Meric, I.; van der Zande, A. M.; Huang, P. Y.; Wang, L.; Muller, D.; Shepard, K. L.; Hone, J. Chemical Vapor Deposition-Derived Graphene with Electrical Performance of Exfoliated Graphene. *Nano Lett.* **2012**, *12*, 2751–2756.
- (27) Zhang, Y.; Brar, V. W.; Girit, C.; Zettl, A.; Crommie, M. F. Origin of Spatial Charge Inhomogeneity in Graphene. *Nat. Phys.* **2009**, *5*, 722–726.
- (28) Hutchinson, J. W.; Suo, Z. Mixed Mode Cracking in Layered Materials. *Adv. Appl. Mech.* **1991**, *29*, 63–191.
- (29) Zabel, J.; Nair, R. R.; Ott, A.; Georgiou, T.; Geim, A. K.; Novoselov, K. S.; Casiraghi, C. Raman Spectroscopy of Graphene and Bilayer under Biaxial Strain: Bubbles and Balloons. *Nano Lett.* **2012**, *12*, 617–621.
- (30) Yan, J.; Zhang, Y.; Kim, P.; Pinczuk, A. Electric Field Effect Tuning of Electron-Phonon Coupling in Graphene. *Phys. Rev. Lett.* **2007**, *98*, 166802.
- (31) Volinsky, A. A.; Moody, N. R.; Gerberich, W. W. Interfacial Toughness Measurements for Thin Films on Substrates. *Acta Mater.* **2002**, *50*, 441–466.
- (32) Havener, R. W.; Liang, Y.; Brown, L.; Yang, L.; Park, J. Van Hove Singularities and Excitonic Effects in the Optical Conductivity of Twisted Bilayer Graphene. *Nano Lett.* **2014**, *14*, 3353–3357.
- (33) Colson, J. W.; Woll, A. R.; Mukherjee, A.; Levendorf, M. P.; Spitler, E. L.; Shields, V. B.; Spencer, M. G.; Park, J.; Dichtel, W. R. Oriented 2D Covalent Organic Framework Thin Films on Single-Layer Graphene. *Science* **2011**, *332*, 228–231.
- (34) MacLeod, J. M.; Rosei, F. Molecular Self-Assembly on Graphene. *Small* **2014**, *10*, 1038–1049.
- (35) Jacobberger, R. M.; Kiraly, B.; Fortin-Deschenes, M.; Levesque, P. L.; McElhinny, K. M.; Brady, G. J.; Delgado, R. R.; Roy, S. S.; Mannix, A.; Lagally, M. G.; Evans, P. G.; Desjardins, P.; Martel, R.; Hersam, M. C.; Guisinger, N. P.; Arnold, M. S. Direct Oriented Growth of Armchair Graphene Nanoribbons on Germanium. *Nat. Commun.* **2015**, *6*, 8006.
- (36) Yin, J.; Liu, X.; Lu, W.; Li, J.; Cao, Y.; Li, Y.; Xu, Y.; Li, X.; Zhou, J.; Jin, C.; Guo, W. Aligned Growth of Hexagonal Boron Nitride Monolayer on Germanium. *Small* **2015**, *11*, 5375–5380.
- (37) Kim, C. J.; Sánchez-Castillo, A.; Ziegler, Z.; Ogawa, Y.; Noguez, C.; Park, J. Chiral Atomically Thin Films. *Nat. Nanotechnol.* **2016**, *11*, 520–524.
- (38) Cao, Y.; Fatemi, V.; Fang, S.; Watanabe, K.; Taniguchi, T.; Kaxiras, E.; Jarillo-Herrero, P. Unconventional Superconductivity in Magic-Angle Graphene Superlattices. *Nature* **2018**, *556*, 43–50.
- (39) Kim, M.; Park, G. H.; Lee, J.; Lee, J. H.; Park, J.; Lee, H.; Lee, G. H.; Lee, H. J. Strong Proximity Josephson Coupling in Vertically Stacked NbSe₂-Graphene-NbSe₂ van der Waals Junctions. *Nano Lett.* **2017**, *17*, 6125–6130.
- (40) Son, J.; Kwon, J.; Kim, S. P.; Lv, Y.; Yu, J.; Lee, J. Y.; Ryu, H.; Watanabe, K.; Taniguchi, T.; Garrido-Menacho, R.; Mason, N.; Ertekin, E.; Huang, P. Y.; Lee, G. H.; van der Zande, A. M. Atomically Precise Graphene Etch Stops for Three Dimensional Integrated Systems from Two Dimensional Material Heterostructures. *Nat. Commun.* **2018**, *9*, 3988.